Insights into sequential hydro-shearing stimulation along a wellbore in the context of Haute-Sorne

Geo-energy Lab, EPFL

September 2024

1 Problem setup:

We consider two circular fractures, each with a radius of 300 meters, separated by a vertical distance of 40 meters. The fractures are assumed to be homogeneous, isotropic, and linear elastic rock masses. Fracture plane is governed by Coulomb's friction with a slip-weakening friction coefficient. The fractures are considered to be impermeable signifying that there is no leak-off.

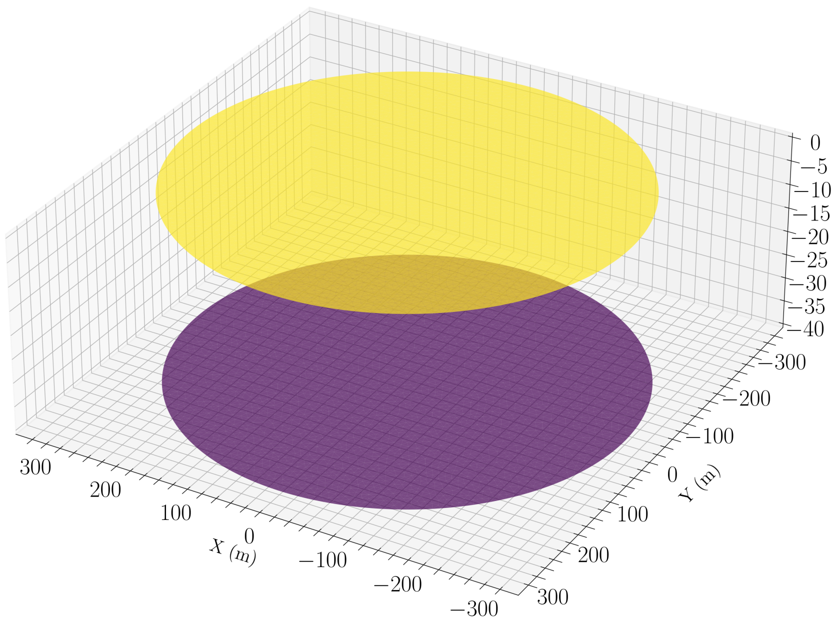

Figure 1: Two circular fractures of 300 m radius separated by a distance of 40 m

For the in-situ stress state, we rely on the dataset of the Basel project, providing stress gradients at a depth of 5000 meters. The principal stresses at this depth are as follows: $S_1 = S_H = 162$ MPa, $S_2 = S_v = 124.5$ MPa, and $S_3 = S_h = 85$ MPa. The azimuth of the maximum horizontal stress $S_1 = S_H$ is oriented N144°E.

This state of principal stresses results in the following local stress tensor, expressed in the local easting-northing-elevation coordinate system (x, y, z), with compressive stresses considered positive:

$$\sigma = \begin{bmatrix} 111.6\,\text{MPa} & -36.6\,\text{MPa} & 0 \\ -36.6\,\text{MPa} & 135.4\,\text{MPa} & 0 \\ 0 & 0 & 124.5\,\text{MPa} \end{bmatrix}$$

Assuming the water table is at ground level, the resulting pore pressure is $p_0 = 49.05$ MPa. Based on this pore pressure, the effective stresses are calculated. A Mohr's circle analysis is performed to identify the plane closest to failure, which is then selected for further analysis.

On the most susceptible plane, the effective normal stress is $\sigma'_0 = 51.13$ MPa, and the shear stress is $\tau_0 = 30.64$ MPa.

The following injection schedule is considered:

Time (hours)	Injection Rate (L/min)
0-2	10
2-4	20
4-6	45
6-10	60

2 Results from Axisymmetric simulation:

We conduct an axisymmetric simulation of fluid injection into the first fracture. The axisymmetric setup offers computational efficiency, enabling rapid simulations that facilitate timely engineering decisions. The primary objective of this simulation is to estimate the rupture radius resulting from the specified injection scheme and to assess the corresponding stress transfer or induced stress in the adjacent subsidiary fracture at the conclusion of the injection process.

The parameters used in the model are tabulated below:

Parameters	Value
Young's modulus (E)	40 GPa
Poisson's ratio (ν)	0.0
Peak friction coefficient (f_p)	0.63
Residual friction coefficient (f_p)	0.6
Dilatancy coefficient (f_d)	0.1
Critical slip distance (d_c)	$1 \times 10^{-2} m$
Rock hydraulic diffusivity	$0.08\ m^2/s$
Normal effective traction (σ'_0)	51.13 MPa
Shear effective traction (τ_0)	30.64 MPa
Hydraulic aperture (w_h)	4.93×10^{-5} m
Dynamic viscosity (μ)	2.5×10^{-4} Pa-s
Hydraulic Transmissivity (K)	$1 \times 10^{-14} m^3$
Storage coefficient	$5 \times 10^{-10} 1/Pa$
Domain radius (L)	300 m
Number of elements (N_{elem})	1000

Table 1: Parameters used in the axisymmetric simulation

Figure 2a illustrates the injection overpressure during the injection process, with the maximum overpressure reaching 12 MPa. Furthermore, utilizing this parameter set and the specified injection scheme, a rupture radius of 124.6 meters is obtained, as depicted in Figure 2b. In addition, Figure 3 presents the increase in hydraulic transmissivity within the rupture zone, depicting a two-order-of-magnitude enhancement at the wellbore.

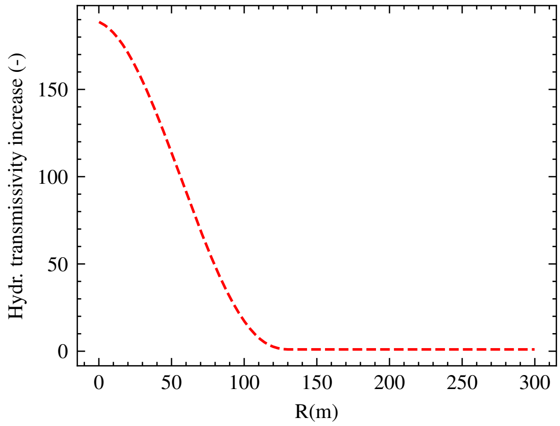

Figure 3: Increase of hydraulic transmissivity (in multiples of the initial transmissivity)

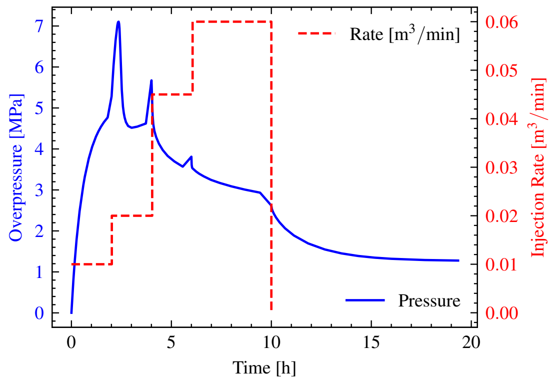

(a) Injection rate (in red) and the corresponding overpressure (in blue)

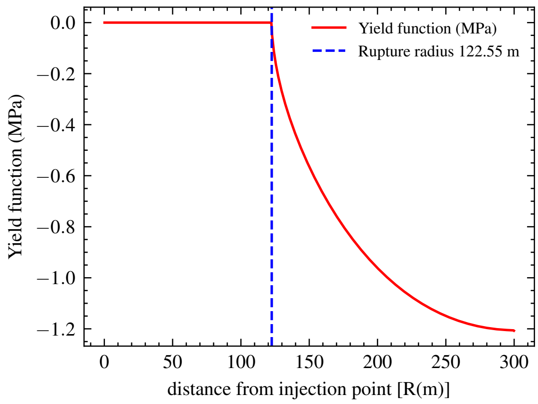

(b) Yield function after 10 hours of injection

Figure 2

The primary objective is to analyze whether any stress transfer occurs to the subsidiary fracture, which is separated by a distance d, following the completion of injection into the first fracture. To investigate this, we compute the stress transferred to the second fracture, located 40 meters vertically from the first one. To analyse this, the displacement discontinuities obtained at the conclusion of the injection into the first fracture are projected onto a circular mesh, which serves as the basis for a three-dimensional model of the problem. Subsequently, a boundary element hierarchical matrix (H-matrix) is constructed, corresponding to the simulation parameters and the circular mesh. Using this H-matrix and the local displacement discontinuities projected onto the mesh, we calculate the stress induced on the subsidiary fracture.

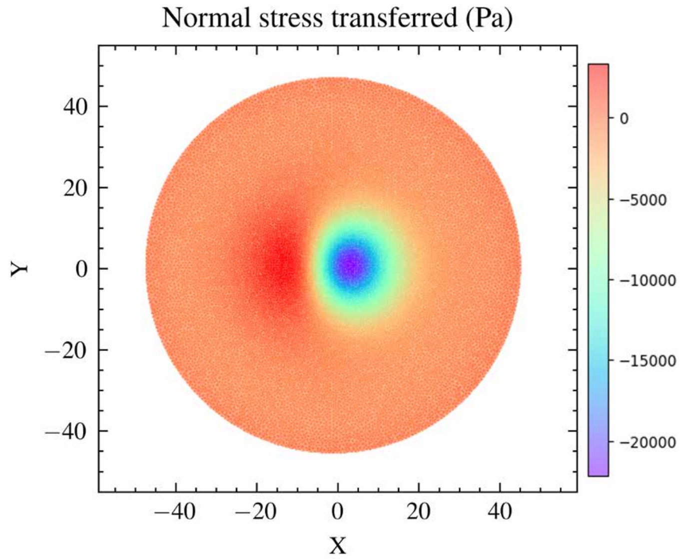

Figure 4: Normal stress transferred onto the second fracture after the end of injection into the first fracture

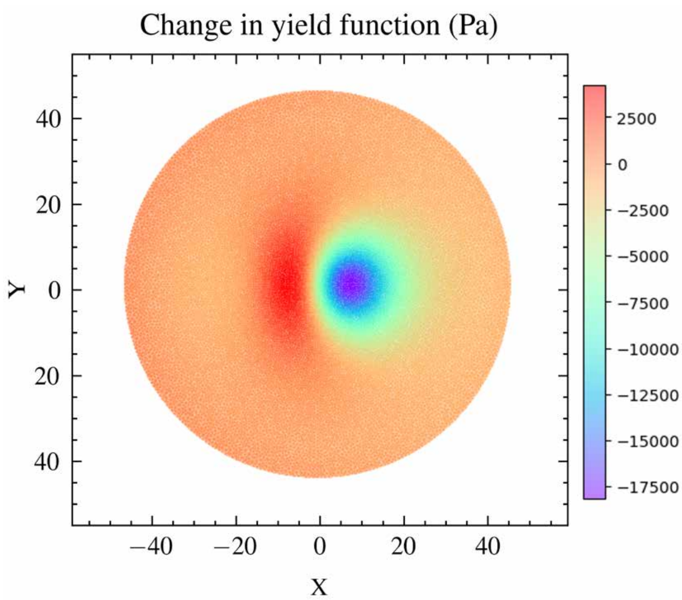

Figure 5: Change in yield function of the second fracture after the end of injection into the first fracture

Figure 4 illustrates the transferred normal stress onto the second fracture after the completion of injection into the first fracture. The corresponding change in the yield function of the second fracture is depicted in Figure 5. It is evident that some regions of the second fracture exhibit increased strength, while others show a reduction in strength compared to the initial state. The increase in strength in certain areas is likely due to the opening of the first fracture, which results in an increase in compressive normal stress on the second fracture. Out of 11,972 elements, 3835 elements exhibited an increase in strength, accounting for approximately 32% of the fracture area. The maximum increase in the yield function is 0.175 MPa, while the maximum decrease is 0.025 MPa. Therefore, in both cases, the magnitude of stress transfer is relatively small compared to the initial stress state. This magnitude of stress transfer will decrease even further for the subsequent fractures.

3 Example simulation in PyFracX for multi-stage injection in 3D:

This example presents the results of a multi-stage injection simulation into two parallel fractures in a three-dimensional setup to demonstrate the capabilities of the solver. We consider two circular parallel fractures, each with a radius of 50 meters, separated by a vertical distance of 20 meters. The fractures are discretized using a mesh of 62,360 triangular elements. The fractures are assumed to be homogeneous, isotropic, and composed of linear elastic rock masses. The fracture planes are governed by Coulomb's friction law with a slip-weakening friction coefficient. Fractures are subjected to a uniform initial stress state, characterized by normal stress σ_0 and shear stress τ_0.

Initially, fluid is injected at a point source located at the center of the first fracture along the z-axis. This injection phase lasts for 300,000 seconds (3.47 days) and is immediately followed by injection into the second fracture, which continues for 400,000 seconds (4.72 days) under similar conditions. The material properties include a Poisson's ratio of $\nu = 0.45$, indicating that the rupture profile is elliptical. The rock masses are considered impermeable, implying that no fluid leak-off occurs during the process. The injection schedule is illustrated in Figure 7a.

Parameters	**Value**
Young's modulus (E)	78 GPa
Poisson's ratio (ν)	0.3
Peak friction coefficient (f_p)	0.6
Residual friction coefficient (f_p)	0.54
Dilatancy coefficient (f_d)	0.5
Critical slip distance (d_c)	$6.67 \times 10^{-3} m$
Rock hydraulic diffusivity	$0.01\ m^2/s$
Normal effective traction (σ_0')	80 MPa
Shear effective traction (τ_0)	28.88 MPa
Hydraulic aperture (w_h)	3×10^{-4} m
Dynamic viscosity (μ)	8.9×10^{-4} Pa-s
Hydraulic Transmissivity (K)	$2.5 \times 10^{-9} m^2/s$
Storage coefficient	$2.5 \times 10^{-7} m^2/s$
Domain radius (L)	50 m
Number of elements (N_{elem})	62360

Table 2: Parameters used in the multi-stage injection simulation

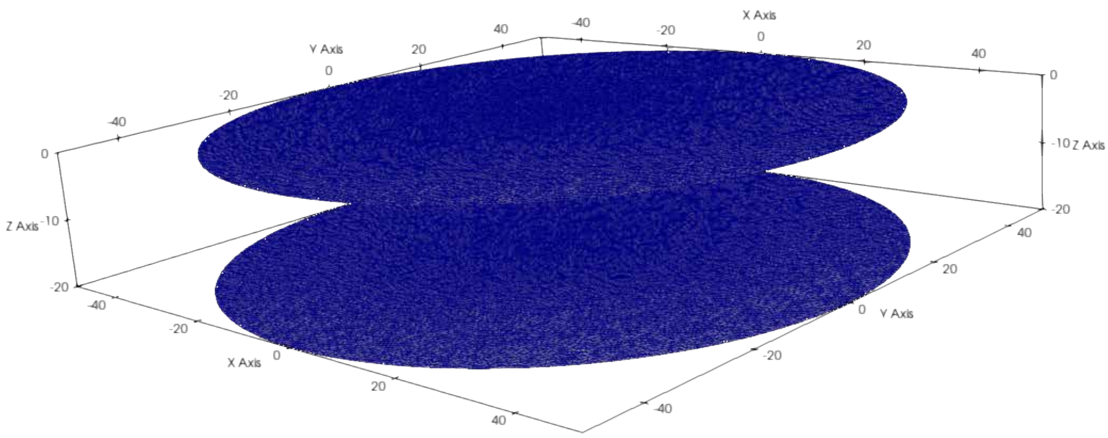

Figure 6: Schematic of the problem domain with two parallel fractures

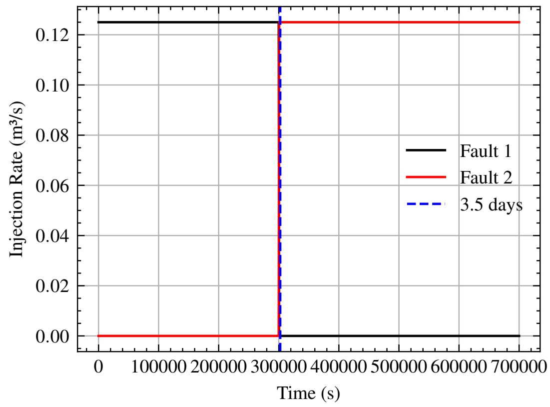

(a) Injection schedule for the multi-stage injection simulation

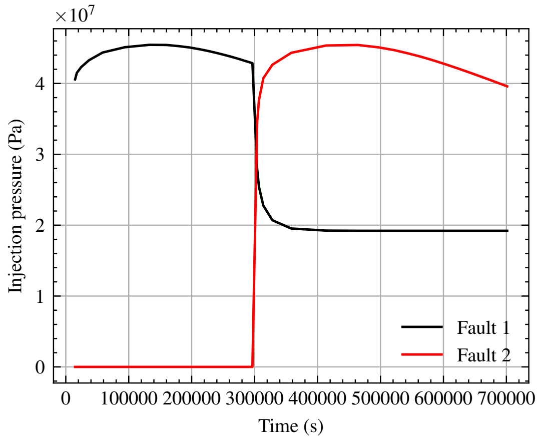

(b) Injection pressure with time on both the fractures

Figure 7

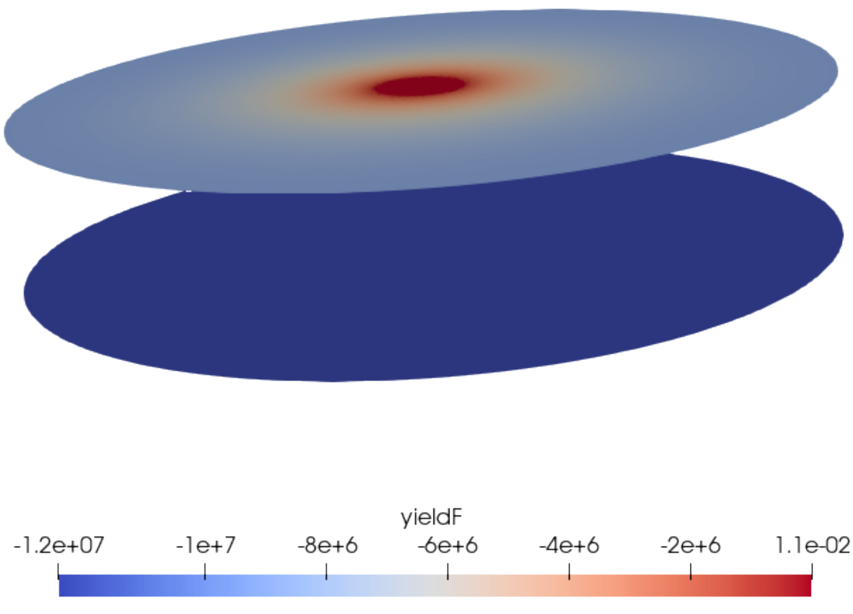

Figure 8: **Yield function(Pa)** at the end of the injection in the first fracture, at t = 300000 s

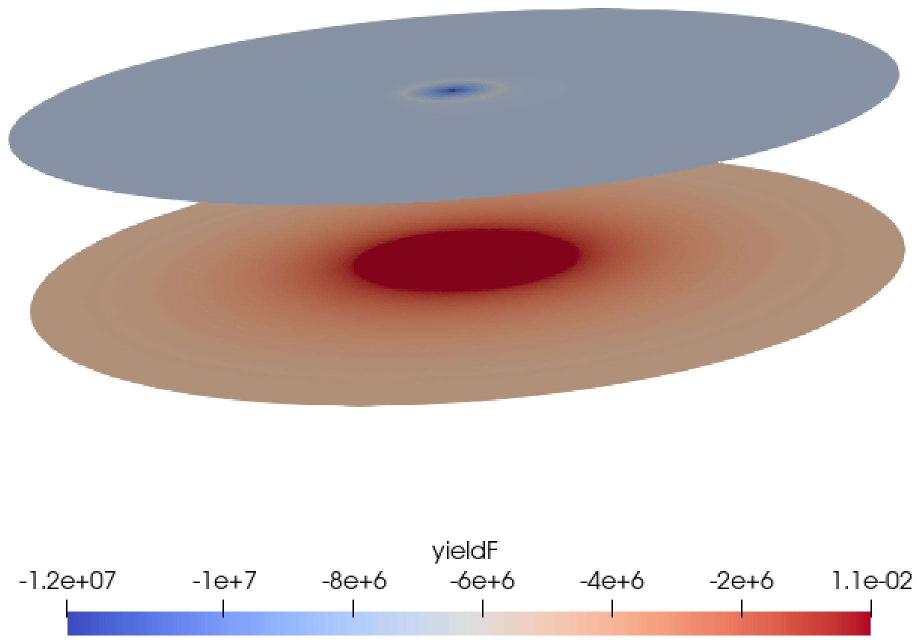

Figure 9: **Yield function (Pa)** at the end of the injection in the second fracture, at t = 700000 s

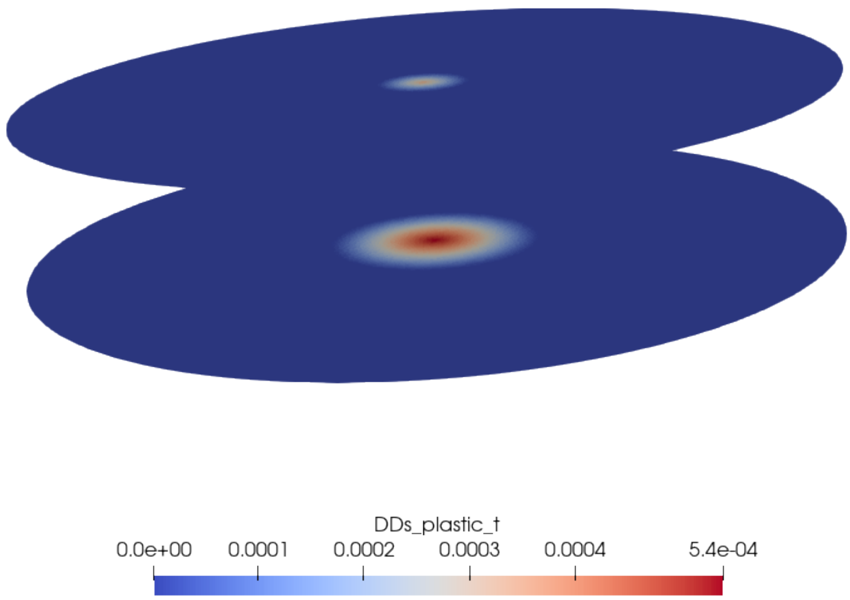

Figure 10: **Plastic slip (m)** obtained at the end of injection, t = 700000 s

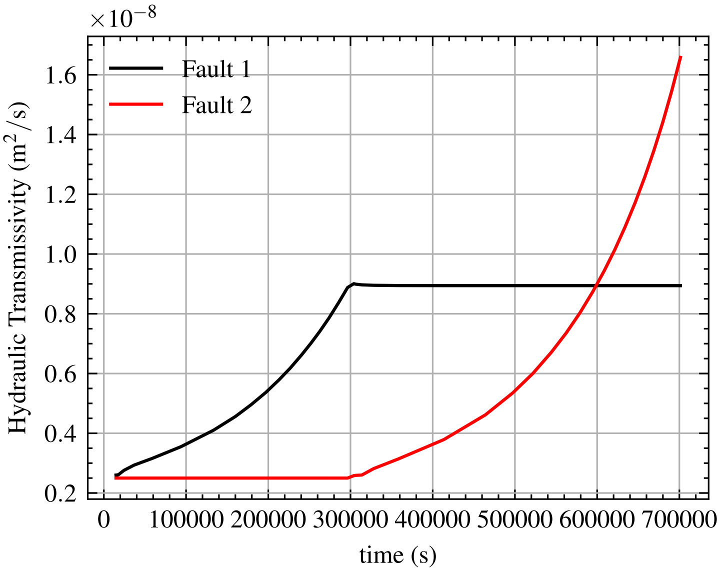

Figure 11: Variation of hydraulic transmissivity at the wellbore in both fractures with time

Figures 8 and 9 illustrate the yield function, which indicates the evolution of the rupture at the end of injection into the first fracture and at the end of injection into the second fracture, respectively. Figure 10 shows the slip distribution obtained after the completion of injection into both fractures. Additionally, Figure 11 reveals a significant increase in hydraulic transmissivity at the wellbore, with a 350% gain in the first fracture and a 640% increase in the second fracture.